

Regulated photo/thermal dual and programmable staged responsive shape memory poly(aryl ether ketone)

Shuai Yang | Yang He | Jinsong Leng 

Center for Composite Materials and Structures, Harbin Institute of Technology, Harbin, People's Republic of China

Correspondence

Jinsong Leng, Center for Composite Materials and Structures, Harbin Institute of Technology, 150080, Harbin, People's Republic of China.

Email: lengjs@hit.edu.cn

Funding information

National Natural Science Foundation of China, Grant/Award Number: 11632005; Heilongjiang Touyan Innovation Team Program

Abstract

In this paper, two types of photo/thermal dual and programmable staged responsive shape memory PAEK are fabricated. On one side, photosensitive cinnamic acid (CA) is grafted onto shape memory poly(aryl ether ketone) (PAEK) chains to obtain PEAK-CA with photo/thermal response. On the other hand, PAEK/CA composites are prepared via a facile physical blending as comparison. Both PAEK-CA and PAEK/CA materials exhibit the excellent heat-triggered (recovery ratio over 91.8%) and photo-responsive shape memory effect (recovery ratio over 76.5%). More interestingly, the staged shape fixity and shape recovery behaviors can be realized by combining independent photo/heat responsive shape memory behaviors. Take the PAEK/CA for example, the irradiation with λ of 365 nm can be used for shape fixity, and shape recovery can be triggered by heating. Meanwhile, the fixation of the temporary shape of the sample can also be realized by heating-cooling process, and then the irradiation with λ of 365 nm is used for shape recovery. These photo/thermal dual and staged responsive shape memory PAEK materials could be widely utilized in fields of soft robots, smart actuators, and deformable devices.

KEYWORDS

photo/thermal dual response, photo/thermal staged response, photosensitive cinnamic acid, shape memory PAEK

1 | INTRODUCTION

As a type of stimulus-responsive smart materials, shape memory polymers (SMPs) have gained attention of researchers due to the unique programming deformation ability which could retain the temporary shape and recover to the original shape upon the external stimulus such as heat,¹ electric,² magnetic,³ and light.⁴ The shape deformation ability, dictated by the transition of internal molecular ordering and phase state,⁵ imparts polymer wide using potential in the fields of aerospace,⁶ actuators,⁷ and smart devices,^{8,9} etc. Among the diverse actuations for SMPs, the heat-triggered SMPs are the earliest fabricated and the most widely used.^{10,11} The molecular chains

of polymer are frozen while the temperature is lower than transition temperature (T_t). Once the temperature reaches up to T_t , the molecular chains begin to thaw, and the sample deforms under the external force. The deformation shape could be retained when it cools. While the temperature reaches to T_t again, the molecular chains melt and recover to the original shape.^{12–15}

Comparing with heat-triggered SMPs, light-triggered SMPs possess wide application prospect due to the remote control, instantaneity, and spatiality.^{13–16} At present, there are two main methods for the fabrication of photo-responsive SMPs: one is the introduction of photosensitive groups, and the other is the incorporation of fillers with photothermal effect.^{17,18} Photosensitive

reactions commonly include photoisomerization, which could occur in azobenzene,^{19–22} spiropyrane groups,^{23,24} and photo-crosslinking reaction, occurring in cinnamic acid groups.^{25–29} Upon the irradiation, the internal structures change accompanying with the occurrence of reactions. In these stage, the intrinsic elasticity of molecular chains dominates the shape recovery behaviors.³⁰ The fillers with photothermal effect mainly contain carbon black,^{31,32} carbon nanotubes,^{33,34} Au nanorods,^{35–37} and polydopamine etc.^{38–40} Upon light irradiation, the fillers transform the light energy into heat, promoting the shape recovery above the temperature of T_t .

Due to the diverse triggering modes, multi-stimuli responsive SMPs have attracted attention at recent years,^{10,41–44} and the incorporation of sensitive groups or fillers into SMP matrix could fabricate the multi-stimuli responsive SMPs. Cinnamic acid (CA), as a kind of universal photo-responsive group, could crosslink under the UV light at $\lambda > 260$ nm, and de-crosslink under the UV light at $\lambda < 260$ nm.⁴⁵ Besides, photo/thermal dual triggered SMPs could be fabricated through the integration of photo-responsive CA into heat-triggered SMPs matrix.^{46,47} In addition, poly(aryl ether ketone) (PAEK), as a type of high-performance thermoplastic, has been widely used in fields of aerospace, storage energy, and actuators,^{48–51} due to the excellent mechanical properties, chemistry resistance, and thermal stability.^{52,53} The flexible and rigid segments in PAEK main chains could be tuned through the arrangement and manipulation of monomers, which impart the great shape memory effect.

In this paper, the chemical grafting PAEK-CA and physical blending PAEK/CA samples were synthesized and characterized via ¹H NMR, FTIR, WAXD, SAXS, UV-vis, DSC, and TGA. Besides, their photo/thermal dual and staged responsive shape memory behaviors were investigated. The prepared PAEK-CA and PAEK/CA composites contributed to their applications in smart deformable devices with excellent photo/thermal response.

2 | EXPERIMENTAL

2.1 | Materials

2,2-Bis(3-amino-4-hydroxyphenyl) hexafluoropropane (BAHFF), 4,4'-difluorobenzophenone (DFBP), potassium carbonate (K_2CO_3), cinnamic acid (CA), dicyclohexylcarbodiimide (DCC), and tetramethylene sulfone (TMSF) were supplied by Aladdin Industrial. Toluene and *N*-methyl kelo-pyrrolidide (NMP) were all bought from Tianjin Guangfu Chemical Reagent Factory.

2.2 | Synthesis of PAEK and PAEK-CA

PAEK was synthesized through a condensation polymerization reported previously.⁵⁴ Certain proportion of BAHFF, DFBP, and K_2CO_3 were added into a 100 mL three-neck flask containing TMSF and toluene, equipped with Dean-Stark trap and nitrogen atmosphere. The temperature of reaction was increased to 140°C for 2 h, to remove the water, and then which was increased to 170°C for 3 h, to carry out the polymerization reaction. After the reaction, the viscous product was poured into a beaker containing large amount of isopropanol. The precipitate was rinsed with deionized water and ethanol for several times, and the synthesized PAEK was dried and stored (yield: 92%).

The PAEK-CA polymer was synthesized by grafting CA onto PAEK backbone. First, certain amount of PAEK and CA were independently dissolved in NMP under stirring. Then, they were blended and vigorously stirred for homogeneous. Afterward, DCC was added into the mixture and continually stirred for 24 h at 50°C. The PAEK-CA solution was precipitated in propanol, and rinsed for several times, and then the product was dried and stored. The molar proportion of PAEK and CA was 1:1 and 1:2, called as PAEK-CA1 and PAEK-CA2, respectively. The synthetic pathway of PAEK-CA was depicted in Scheme 1.

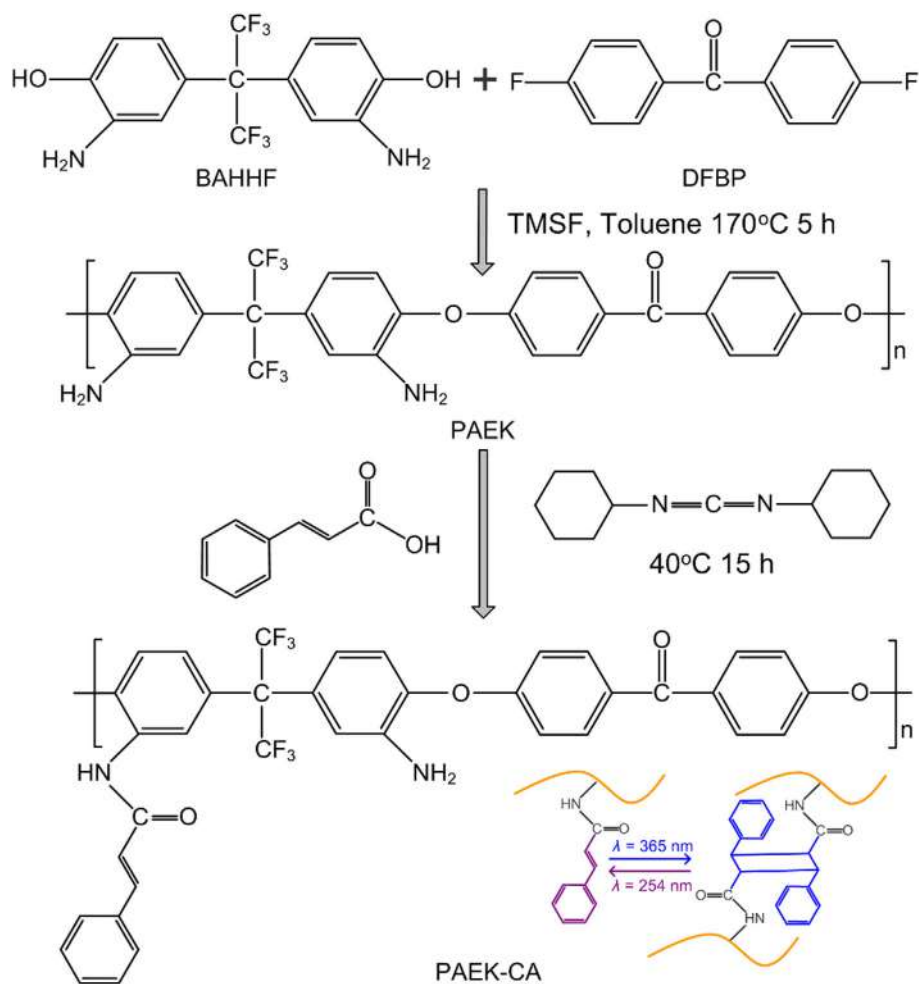
2.3 | Preparation of PAEK, PAEK-CA, and PAEK/CA films

A certain amount of synthesized PAEK and PAEK-CA were independently dissolved into NMP under stirring for 24 h. PAEK and CA were physically blended according to the certain proportion, and the mixture was dissolved into NMP under stirring for 24 h. Then, prepared solutions were cast into a homemade mold and dried at 80°C for 48 h. Afterward, the fabricated films were peeled off and stored carefully. The proportion of PAEK and CA in physical blending was the same with it in grafting reaction, called as PAEK/CA1 and PAEK/CA2, respectively.

2.4 | Characterization

The chemical structures of synthesized PAEK and PAEK-CA were reflected by ¹H-nuclear magnetic resonance (¹H NMR) spectra. $CDCl_3$ was used as the solvent and tetramethylsilane (TMS) was used as the internal reference with an ADVANCE III 400 MHz 010601 spectrometer (Bruker). Fourier transform infrared (FTIR)

SCHEME 1 Synthetic pathway of PAEK-CA. [Color figure can be viewed at wileyonlinelibrary.com]



spectroscopy was revealed by a Spectrum Two (PerkinElmer). Wide-angle x-ray diffraction (WAXD) patterns were performed on an X'pert XRD analyzer (Panalytical B.V.). The 2θ range was 5° – 55° , and a step size was $10^\circ/\text{min}$. Small-angle x-ray scattering (SAXS) spectra was obtained by Shanghai Synchrotron Radiation Facility (BL19U2, SSRF). The scattering vector (q) and the long period (L) of samples could be calculated as following:

$$q = \frac{4\pi \sin \theta}{\lambda} \quad (1)$$

$$L = \frac{2\pi}{q} \quad (2)$$

where q is the scattering vector, λ is the wavelength, 2θ is the scattering angle, and L is the long period of lamellar structures.

UV–visible absorption spectra was recorded using a Mettler-Toledo UV7, and the wavelength range of 200–800 nm. Differential scanning calorimetric (DSC) curves were performed at a temperature range of

25–300°C with a heating rate of $10^\circ\text{C}/\text{min}$, through a DSC 1 STAR System (Mettler-Toledo). Thermal gravimetric analysis (TGA) curves were performed on a TGA/DSC 1 STAR System (Mettler-Toledo). The temperature range was 25–800°C, and the heating rate of $10^\circ\text{C}/\text{min}$.

2.5 | Heat-triggered shape memory test

Heat-triggered shape memory test was conducted via the “U” shape sample test. Film samples with the size of 5 mm × 30 mm were heated up to transition temperature (T_g), and fixed into a “U” shape by a homemade mold. Then, the temperature was cooled down to room temperature, and the temporary “U” shape was obtained. Afterwards, the temperature was increased above T_g again, and the shape recovery could be observed. Digital camera was used to record the recovery process, and the recovery ratio (R_r) and fixity ratio (R_f) were calculated as follows:

$$R_r = \frac{\theta(t) - \theta_0}{180 - \theta_0} \times 100 \quad (3)$$

$$R_f = \frac{180 - \theta_0}{180} \times 100 \quad (4)$$

where θ_0 is the deformation angle at the time of 0 s, and $\theta(t)$ is the deformation angle at the time of t in second.

2.6 | Photo-triggered shape memory test

Photo-triggered shape memory test was carried out via the “M” shape sample test, similarly. Film samples were cut to the size of 5 mm × 30 mm. They were fixed into the “M” shape and treated by UV irradiation with λ of 365 nm for 15 min. Then, the radiated samples were treated with the irradiation at λ of 254 nm for 1 h. After the radiation, the shape recovery of samples could be observed, and captured with a digital camera. The R_f and R_r were calculated from the formula mentioned before.

2.7 | Photo/thermal staged responsive shape memory test

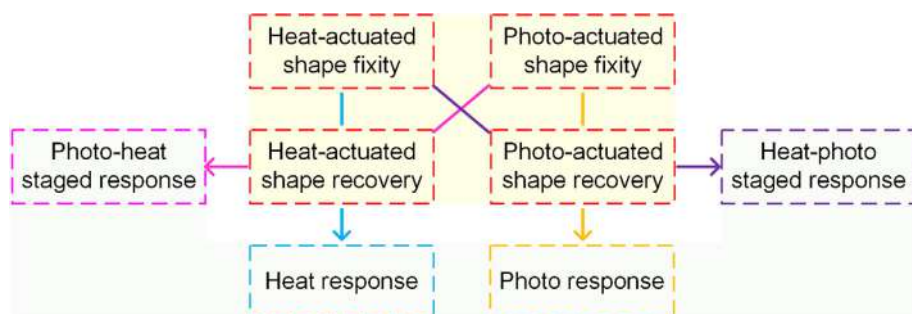
We extracted independent shape fixity and shape recovery behaviors from photo/heat responsive shape memory behaviors, and combined them again for achieving the photo/heat staged responsive shape memory behaviors, shown in Scheme 2.

2.7.1 | Photo-fixity and thermal-recovery

Samples were radiated at λ of 365 nm for 15 min, to fix the temporary shape. Then, they were heated to the transition temperature to recover the original shape.

2.7.2 | Thermal-fixity and photo-recovery

Samples were heated above the T_g to fix the temporary shape. Then, they were treated with the irradiation at λ of 365 nm to achieve the shape recovery.



SCHEME 2 Illustration of photo/heat dual actuated shape memory effect and photo/heat staged actuated shape memory effect. [Color figure can be viewed at wileyonlinelibrary.com]

3 | RESULTS AND DISCUSSION

3.1 | Structure analysis

^1H NMR spectra of synthesized PAEK and PAEK-CA2 is showed in Figure 1a. For PAEK, the chemical shift at 1.58 ppm was corresponding to the protons of amino groups (1). The chemical shifts at 7.07, 7.27, and 7.79 ppm were concerned with the protons of 2, 3, and 4, respectively, which indicated the formation of PAEK backbone. For PAEK-CA2, the chemical shifts of protons in double bonds could be found at 6.40 and 7.70 ppm. The protons on benzene rings were concerned with the chemical shifts at 7.48–7.64 ppm. In Figure 1b, the peak at 3330 cm^{-1} was concerned with the characteristic peak of N–H bonds. The stretching vibration of aryl carbonyl groups was corresponding to the peak of 1593 cm^{-1} , and the peak at 1225 cm^{-1} was attributed to the characteristic peak of aryl ether groups. All these infrared absorptions proved the successful synthesis of target polymers. After the integration of CA monomers, the peak of C=C bonds occurred at 1629 and 1623 cm^{-1} , corresponding to PAEK/CA1 and PAEK-CA1, respectively. In Figure 1c, for PAEK-CA2, after treating at λ of 365 nm, the peak at 1629 cm^{-1} became moderate, concerning with the cycloaddition reaction between double bonds. After irradiating at λ of 254 nm, the de-crosslinking reaction occurred and the peak at 1629 cm^{-1} became sharper as expected. In addition, we characterized chemical structures of the PAEK/CA2 treated by the light with λ of 365 and 254 nm, and the consistent results were obtained, shown in Figure S1. As expected, the peak at 1629 cm^{-1} , corresponding to double bonds, became moderate after the irradiation with λ of 365 cm^{-1} . Then, the peak became sharper again after treating at λ of 254 cm^{-1} . WAXD curves are performed in Figure 1d,e. As shown in Figure 1d, PAEK/CA exhibited the wide and flat diffraction peaks, indicating the semi-crystalline of PAEK and plasticizing effect of CA components. Nevertheless, PAEK-CA exhibited narrow sharp peaks, which could be attributed to that the grafting of CA groups on to PAEK main chains transformed the crystalline phases

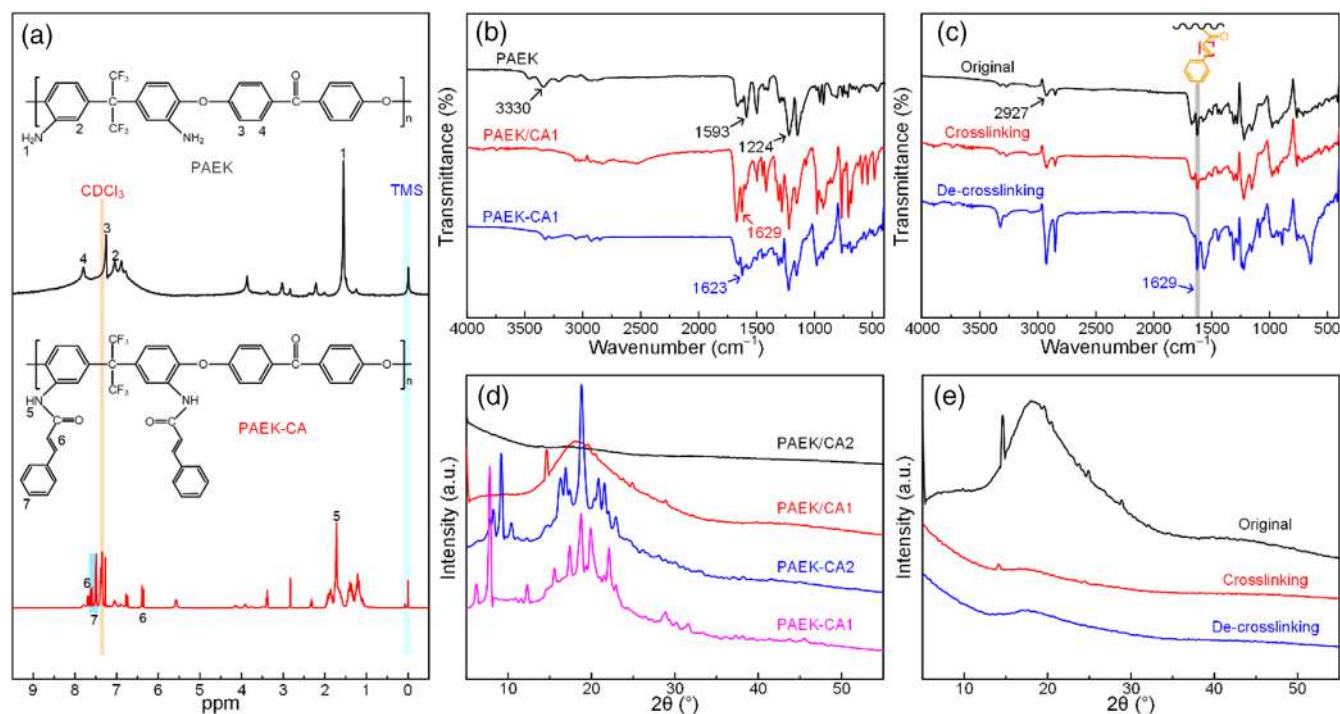


FIGURE 1 (a) ¹H NMR spectra of PAEK and PAEK-C2; FTIR spectra of (b) PAEK, PAEK/CA1, PAEK-CA1; and (c) PAEK-CA2 with the UV treatment (λ of 365 nm and 254 nm); WAXD curves of (d) PAEK/CA and PAEK-CA; and (e) PAEK/CA1 treated at λ of 365 nm and 254 nm. [Color figure can be viewed at wileyonlinelibrary.com]

of original PAEK, and formed the new crystalline phases. In Figure 1e, after the irradiation, the crystalline of PAEK/CA1 decreased, which was concerned with the cycloaddition and de-crosslinking reaction. Nevertheless, upon the irradiation, the crystalline of PAEK-CA1 did not exhibit the significant difference, depicted in Figure S2.

2D SAXS patterns, 1D integral curves, and the long period, q_{\max} statistical chart are showed in Figure 2. In Figure 2a, all the prepared PAEK showed the similar diffuse scattering feature, which was circular and surrounded the beam spot. The intensity of scattered signals was slightly different, which exhibited non-regular. There were not any direct connections between the proportion of CA monomers and the internal micro-structure. In Figure 2b, all the prepared PAEK showed the same q_{\max} , which could indicate that the internal micro-structure had no difference among the various proportions of prepared PAEK. According to Bragg's law, the long period (L) was calculated. The unified value implied the similar distribution of internal crystalline lamellae. Figure 2c shows the 2D SAXS patterns of PAEK/CA1 film treated at λ of 365 and 254 nm. We could observe that there was not significant transformation on scattering fringes while crosslinking and de-crosslinking. Meanwhile, the q_{\max} value and long period did not exhibit any difference (shown in Figure 2d), which could be attributed to that

the crosslinking and de-crosslinking reaction among CA groups, occupied as fillers, could not transform the internal crystalline lamellae. Nevertheless, for the CA-grafting system, the reaction among CA groups significantly transform the distance between adjacent molecular chains. Thus, in crosslinking and de-crosslinking process, the q_{\max} value increased firstly, and decreased subsequently, indicating that the long period decreased firstly, and decreased subsequently, depicted in Figure S3.

UV-visible absorption spectra of PAEK/CA2, PAEK/CA1, PAEK-CA2, and PAEK-CA1 upon the diverse irradiated time at λ of 365 nm and 254 nm are showed in Figure 3a-c. In Figure 3a, we could observed that all the prepared samples exhibited obvious characteristic peaks at 280 nm, corresponding to the photosensitive CA groups. In Figure 3b, while treated at λ of 365 nm, double bonds cracked and the cycloaddition reaction occurred, and the absorbed peak at 280 nm decreased. Increasing the treated time, the absorption peak became lower. In Figure 3c, after irradiating at λ of 365 nm and 254 nm, the de-crosslinking reaction occurred, and double bonds formed again. As a result, the adsorbed peak at 280 nm increased. Meanwhile, as the increasing of treated time, the peak at 280 nm became sharper. Figure S4 shows different treated time at λ of 365 nm and 254 nm on PAEK-CA2 film. In Figure S4a, increasing the treated time at λ of 365 nm, the peak at 280 nm became lower. Nevertheless, increasing

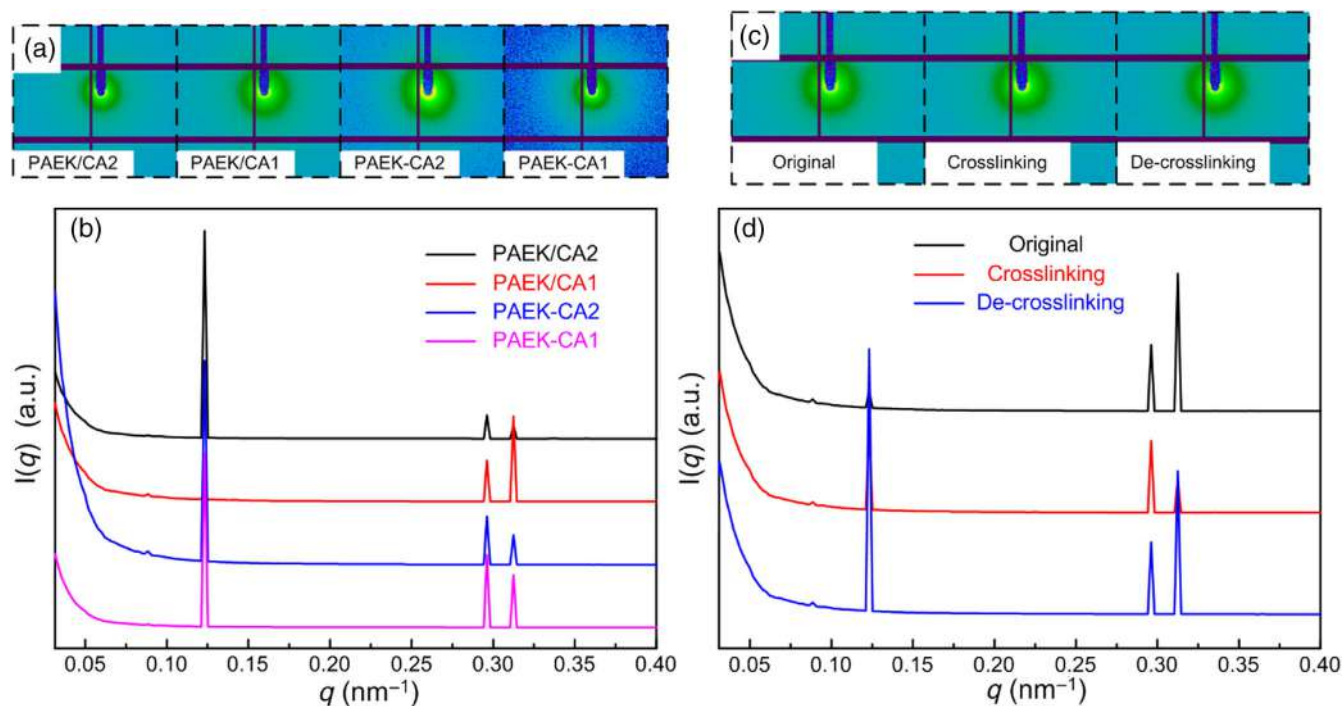


FIGURE 2 (a) 2D SAXS patterns and (b) 1D integral curves of PAEK/CA and PAEK-CA; (c) 2D SAXS patterns and (d) 1D integral curves of PAEK/CA1 treated with UV irradiation with λ of 365 and 254 nm, respectively. [Color figure can be viewed at wileyonlinelibrary.com]

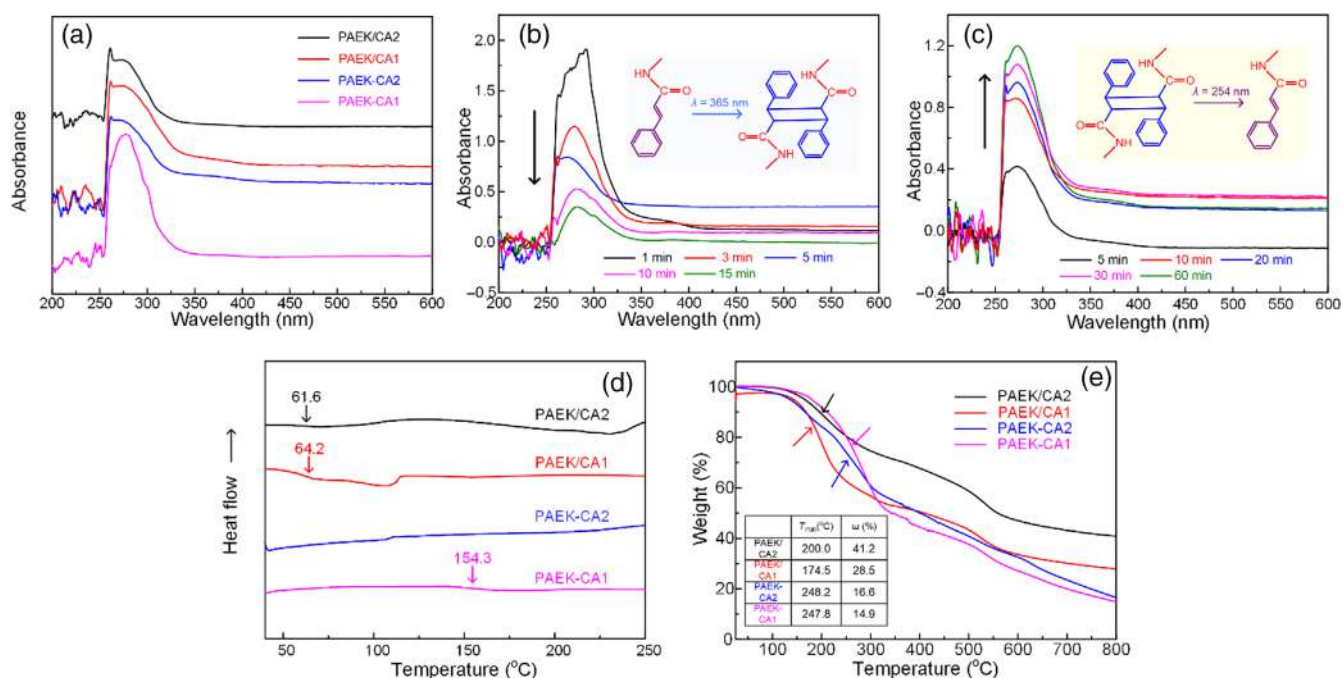


FIGURE 3 UV-visible absorption spectra (a) PAEK/CA2, PAEK/CA1, PAEK-CA2, and PAEK-CA1; (b) Different treated time with the irradiation at λ of 365 nm on PAEK/CA2; (c) Different treated time with the irradiation at λ of 365 and 254 nm on PAEK/CA2; (d) DSC curves of PAEK/CA2, PAEK/CA1, PAEK-CA2, and PAEK-CA1; (e) TGA curves of PAEK/CA2, PAEK/CA1, PAEK-CA2, and PAEK-CA1. [Color figure can be viewed at wileyonlinelibrary.com]

the treated time at λ of 254 nm, the peak became shaper again, depicted in Figure S4b. Figure 3d shows DSC curves of PAEK/CA2, PAEK/CA1, PAEK-CA2, and PAEK-CA1.

CA monomers, acted as plasticizer, would decrease the T_g of PAEK. We could observed that the T_g of PAEK/CA2 was 61.6°C, and the T_g of PAEK/CA1 was 64.2°C.

Nevertheless, while grafting CA groups onto PAEK main chains, the chains entanglement became more intense, promoting the increasing of T_g . There was not obvious peak found for the PAEK-CA2 chains, which might be concerned with the intense accumulation of PAEK chains, and the T_g of PAEK-CA1 was 154.3°C. Figure 3e shows the TGA curves of PAEK/CA2, PAEK/CA1, PAEK-CA2, and PAEK-CA1. In Physical blending systems, the initial degradation temperature (T_i) of PAEK/CA2 was 200°C, higher than which of PAEK/CA1 (174.5°C). The residual mass (ω) of PAEK/CA2 at 800°C was 41.2%, more than which of PAEK/CA1 (28.5%). CA monomers, as a kind of small molecule, possess the higher phenyl content than PAEK molecular chains, which promoting the improvement of thermal stability. Similarly, for chemical grafting systems, the T_i of PAEK-CA2 was 248.2°C, higher than which of 247.8°C. The ω of PAEK-CA2 was 16.6%, more than which of PAEK-CA1 (14.9%). The T_i of physical blending PAEK/CA was lower than chemical grafting PAEK-CA, which was concerned with that the grafting of

CA onto PAEK chains increased the intrinsic thermal stability. Nevertheless, the ω of PAEK/CA was higher than PAEK-CA, which was attributed to the higher phenyl content of CA monomers.

3.2 | Heat-actuated shape memory behaviors

Heat-actuated shape memory behaviors of PAEK/CA and PAEK-CA film samples are showed in Figure 4. In Figure 4a, PAEK/CA1 film could finish the whole shape recovery behaviors within 12 s at the temperature of 75°C ($T_g + 10^\circ\text{C}$). In Figure 4b, the recovery ratio of PAEK/CA2 film was the highest, of 96.5%. The recovery ratio of PAEK/CA1 and PAEK-CA1 film was 93.2% and 93.5%, respectively. The recovery ratio of PAEK-CA2 was the lowest of 91.8%. In the physical blending systems, CA monomers acted as the plasticizer, which were conducive to the flexibility of composites and movement

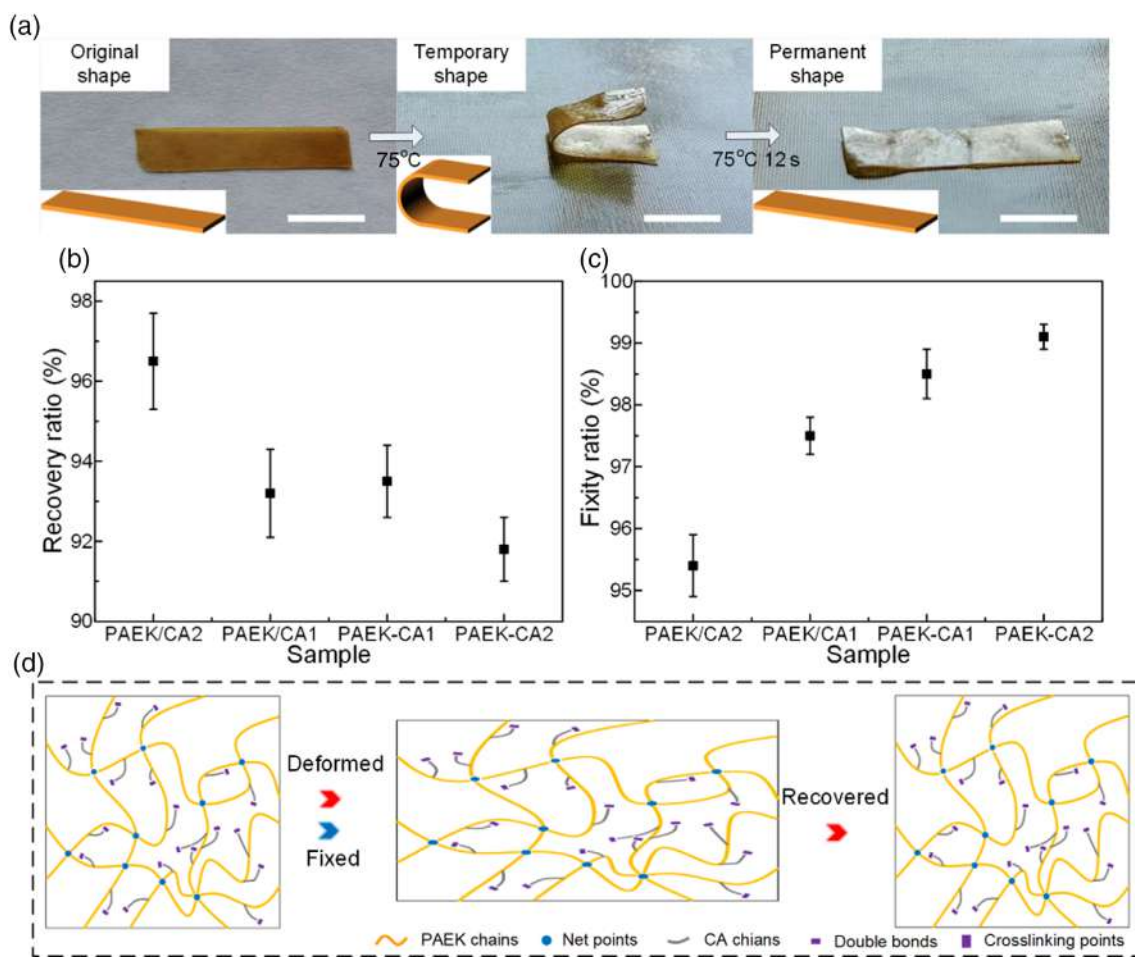


FIGURE 4 Heat-actuated shape memory effect of PAEK/CA and PAEK-CA film samples: (a) The whole shape memory process of PAEK/CA1 film; (b) Recovery ratio; (c) Fixity ratio; (d) Shape memory mechanism of PAEK-CA (Scale bars of 1 cm). [Color figure can be viewed at [wileyonlinelibrary.com](https://onlinelibrary.wiley.com)]

of polymer system, promoting the shape recovery. As the increasing of CA content, the plasticizing effect enhanced, improving the shape recovery ability. In chemical grafting systems, the incorporation of CA improved the flexibility of PAEK molecular chains. Nevertheless, the entanglement of PAEK main chains and CA side groups became more intense, adverse to the movement of molecular chains. In Figure 4c, all the film samples exhibited the high shape fixity ratio, over 95%. The fixity ratio of PAEK-CA films was higher than it of PAEK/CA films. Figure 4d shows the mechanism of heat-actuated shape memory behaviors. Due to the intrinsic thermoplastic, physical entanglements of molecular chains and crystalline phase were as the permanent “net points,” which determined the stationary and recovery of permanent shape. Flexible segments of molecular chains were acted as the reversible phase, which could deformed and fixed to

the temporary shape. Through the heating-deformation, cooling-fixation, and heating-recovery, sample films exhibited heat-actuated shape memory behaviors.

3.3 | Photo-actuated shape memory behaviors

Figure 5 showed the photo-actuated shape memory behaviors of PAEK/CA1 film. In Figure 5a, the horizontal linear shape was as the permanent shape, and in this stage, adjacent CA components maintained mutual independence, where the double bonds were complete. After treating at λ of 365 nm, the double bonds in CA components cracked and reacted with other double bonds in adjacent CA components, to form the crosslinking architecture. During this process, the temporary “M” shape

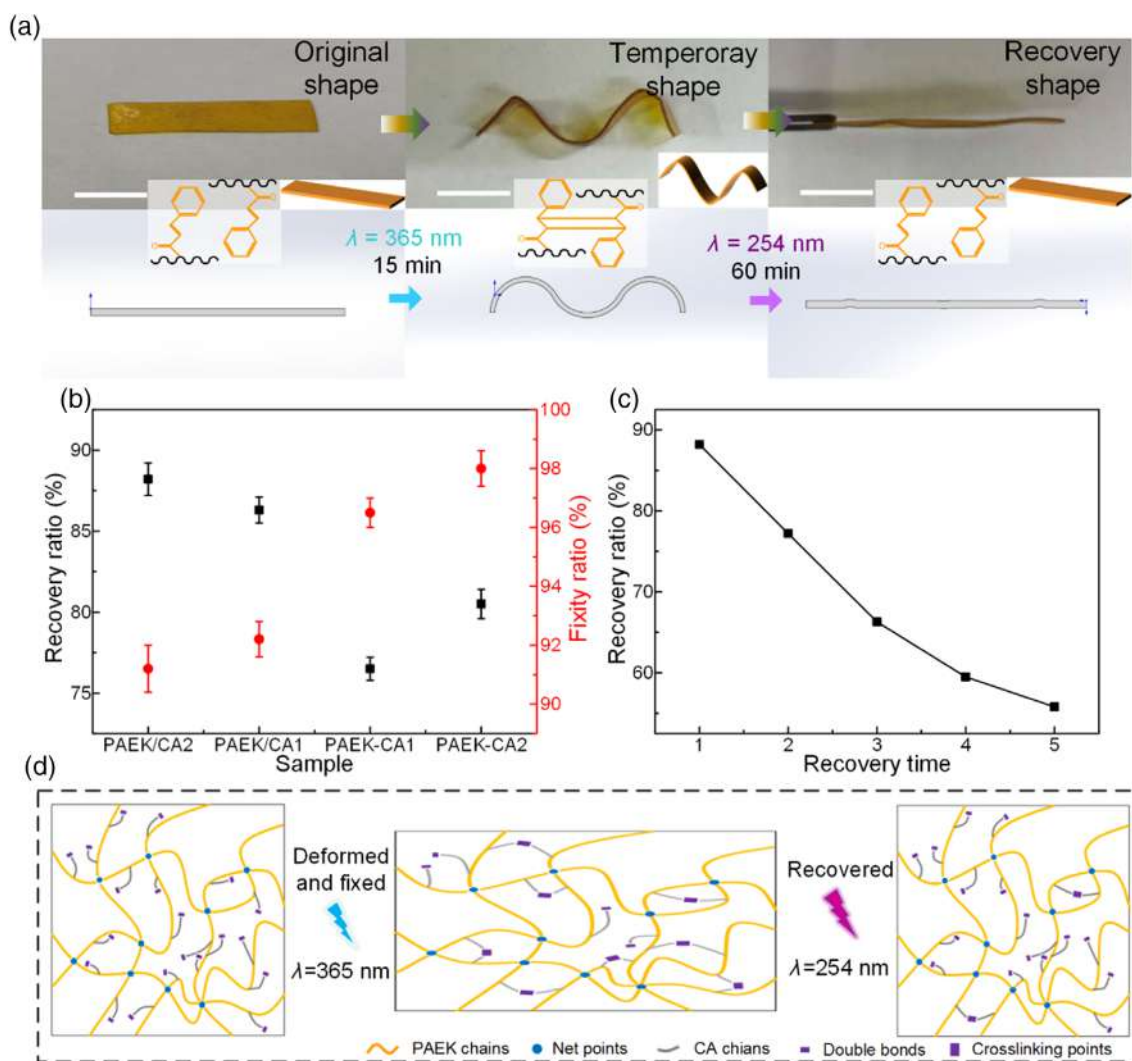


FIGURE 5 Photo-actuated shape memory behaviors of PAEK/CA and PAEK-CA film samples: (a) The whole shape memory process of PAEK/CA1 film; (b) Recovery ratio; (c) Fixity ratio; (d) Shape memory mechanism of PAEK-CA (Scale bars of 1 cm). [Color figure can be viewed at wileyonlinelibrary.com]

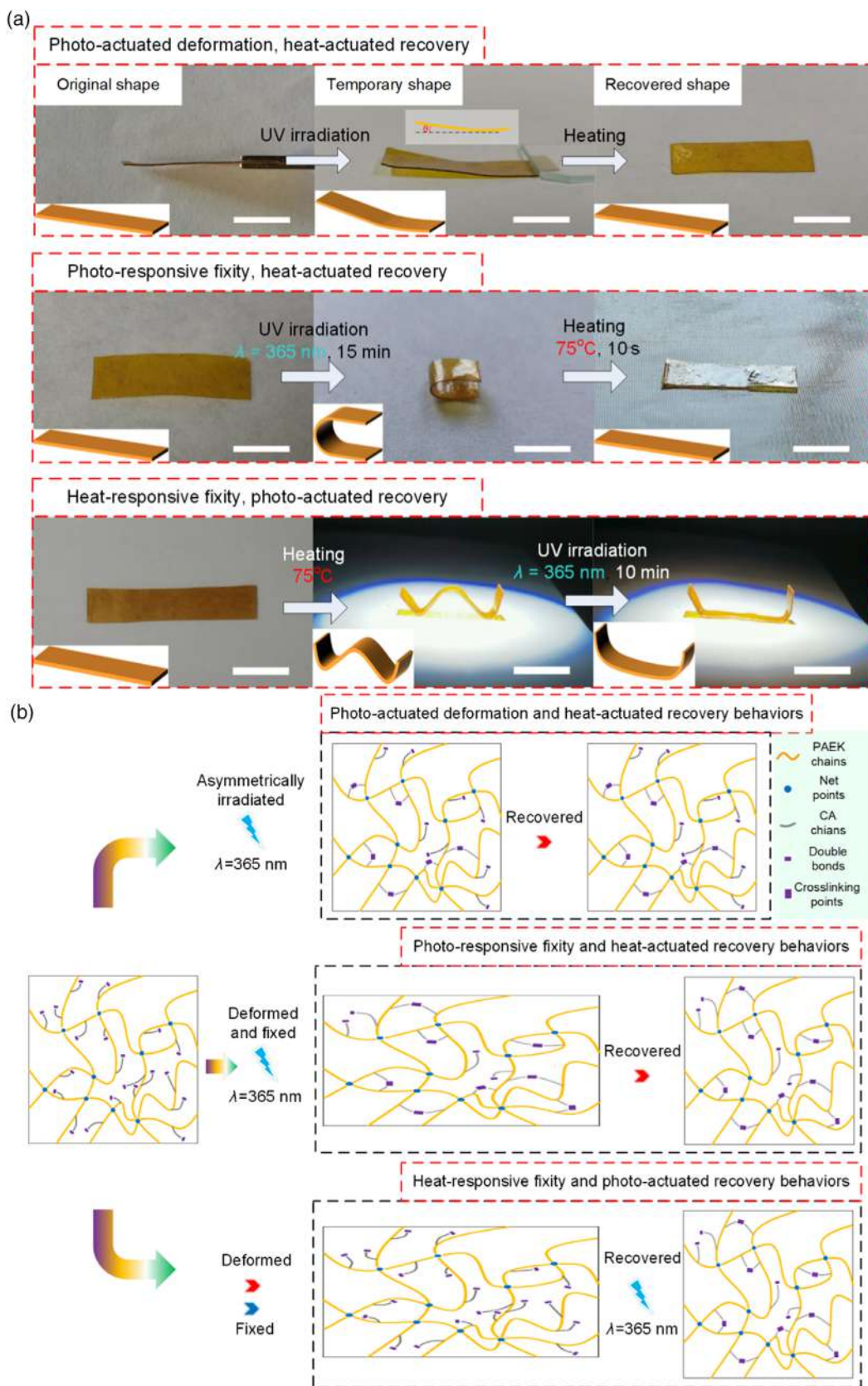


FIGURE 6 Photo/thermal staged responsive shape memory behaviors of PAEK/CA1 films: (a) Photo-actuated deformation and heat-actuated recovery, photo-responsive fixity and heat-actuated recovery, and heat-responsive fixity and photo-actuated recovery behaviors; (b) Shape fixation and recovery mechanisms of PAEK-CA (Scale bars of 1 cm). [Color figure can be viewed at wileyonlinelibrary.com]

was imparted by the external force. Afterwards, the temporary “M” shape sample was irradiated at λ of 254 nm for 60 min. At intervals, we could observe that the “M” shape sample “collapsed”, which gradually tended to horizontal. Ultimately, the shape recovered to the permanent linear shape. In this stage, the formed crosslinking architecture undid to form the independent double bonds. The internal stress stored before was released and the shape recovery occurred spontaneously. Figure 5b shows the photo-actuated shape memory effect of PAEK/CA and PAEK-CA films. The recovery ratio of PAEK/CA1 was 86.3%, and which of PAEK/CA2 was 88.2%. The increasing of CA content quantitatively increased the photosensitive groups, promoting the shape recovery behaviors. Nevertheless, when the CA groups were excess, non-grafted and non-crosslinked groups increased correspondingly, which hindered the movement of molecular chains, detrimental to the spontaneous shape recovery. The recovery ratio of PAEK-CA1 was 76.5%, and which of PAEK-CA2 was 80.5%. The movement of PAEK molecular chains weakened after grafting CA components, which was attributed to the entanglement of adjacent molecular chains. In a comparison with physical blending PAEK/CA composites, chemical grafting PAEK-CA molecular chains were more difficult to move, resulting in the decreasing of recovery ratio. Figure 5c shows the recovery ratio of PAEK/CA1 film after five times of consecutive shape memory processes. After five times of consecutive shape memory process, the recovery ratio decreased from 88.2% to 55.8%. In photo-actuated shape fixity and recovery process, the reaction extent of photo-sensitive crosslinking and de-crosslinking reaction could

not reach up to 100%. Non-crosslinking double bonds and non-de-crosslinking quaternion rings increased, decreasing the extent of reversible addition reaction, which was detrimental to the shape recovery. In Figure 5d, after the irradiation at λ of 365 nm, double bonds of CA components cracked, and the cycloaddition reaction occurred between the adjacent double bonds. In this process, the temporary shape could be obtained by external force and fixed. Afterward, when the irradiation at λ of 254 nm, the de-crosslinking reaction occurred, and the crosslinking cyclic structures were opened, forming the original independent double bonds. In this process, the internal stress stored before was released, and shape recovery occurred.

3.4 | Photo/thermal staged responsive shape memory behaviors

Figure 6a shows the photo/thermal staged responsive shape memory behaviors of PAEK/CA1 films. In the first type of photo-actuated deformation and heat-actuated recovery process, upon the irradiation, the crosslinking reaction between the adjacent CA components preferentially took place on the side with irradiation (upper surface), and almost CA components below did not respond to irradiation. The stress difference between upper and lower surface made the film bend upward. Then, heating the bended film, it could recover to the original shape. As for the second type of photo-actuated fixity and heat-actuated recovery behaviors. First, the film was irradiated at λ of 365 nm for 15 min to enable the programming of the

		Heat response	Photo response	Photo-def Heat-rec	Photo-fix Heat-rec	Heat-fix Photo-rec
Recovery ability		≥ 91.8%	≥ 76.5%	Excellent	Excellent	Good
Fixity ability		≥ 95%	≥ 91.2%	None	Good	Excellent
Temporary shape	External force	✓	✓	✗	✓	✓
	Stimuli	Heat ▶	Photo ⚡	Photo ⚡	Photo ⚡	Heat ▶
	Mechanism	Glass transition				Glass transition
Original shape	Stimuli	Heat ▶	Photo ⚡	Heat ▶	Heat ▶	Photo ⚡
	Time	12s	60min	Rapid	10s	10min
	Mechanism	Glass transition		Glass transition	Glass transition	
Classification		Photo/heat dual response		Photo/heat staged response		

FIGURE 7 Summary of the photo/heat dual and staged responsive shape fixation and recovery behaviors by combining independent photo/thermal shape memory effect (def-deformation; rec-recovery, and fix-fixity). [Color figure can be viewed at wileyonlinelibrary.com]

temporary shape by the external force. Then, the heating of sample to 75°C resulted in the shape recovery within 10s. As for the third type of heat-actuated fixity and photo-actuated recovery behaviors, the film was firstly heated and deformed into the temporary shape by external force. Then, it was irradiated at λ of 365 nm, and the shape recovery could be triggered. Nevertheless, the bended surfaces on the two side of film due to the less irradiation, could not recover to the permanent shape, which indicated that the shape recovery of the film treated with irradiation was based on the photosensitive reaction, not radiant heating. Figure 6b shows the mechanism of photo/heat staged responsive shape memory effect, which was just the combination of heat-actuated shape fixation, shape recovery with photo-actuated shape fixation, shape recovery. While the film sample was treated with asymmetric irradiation at λ of 365 nm, the crosslinking reaction between the adjacent CA components preferentially took place on the side with irradiation, but other CA components did not respond to irradiation. The stress difference imparted film spontaneous bending deformation. Then, it recovered to the permanent shape triggered by heating. During the photo-responsive fixation, the cycloaddition reaction occurred and the temporary shape could be obtained by external force and fixed. Then, the film was heated, and shape recovery occurred. Meanwhile, the temporary shape of film could also be obtained by heating and external force. Then, shape recovery could be triggered by the irradiation at λ of 365 nm. These photo-responsive fixity, heat-actuated recovery and heat-responsive fixity, photo-actuated recovery behaviors could be concluded into photo/heat staged responsive shape memory behaviors.

The fabricated PAEK/CA and PAEK-CA materials both exhibited the excellent heat-triggered shape memory effect and photo-triggered shape memory effect. Besides, we achieved the photo/heat staged responsive shape memory behaviors through extracting the independent shape fixity and recovery process, and combing them again. We summarized these interesting photo/heat dual and staged responsive behaviors, which illustrated in Figure 7. These unique staged responsive shape memory behaviors opened doors for the functionalization designing of the multi-responsive smart materials.

4 | CONCLUSIONS

In this paper, we reported a facile strategy for the fabrication of photo/thermal dual and staged responsive shape memory PAEK. Photosensitive CA groups were grafted onto PAEK chains via conventional condensation polymerization and physically blending to impart the photo-response property. After irradiating at λ of 365 nm, the double bonds in CA groups cracked and the cycloaddition occurred. As the

increasing of exposure time, the crosslinking degree gradually increased. On the other side, after irradiating at λ of 254 nm, de-crosslinking reaction occurred, and double bonds formed again. More importantly, the fabricated PAEK-CA and PAEK/CA materials exhibited photo/heat staged responsive shape memory effect, including photo-responsive shape deformation and heat-triggered shape recovery, photo-responsive shape fixity and heat-triggered shape recovery, even heat-triggered shape fixity and photo-responsive shape recovery behaviors. We believed these photo/heat dual responsive and photo/heat staged responsive shape memory PAEK materials possessed the great potential in fields of soft robots, smart actuators, and deformable devices.

AUTHOR CONTRIBUTIONS

Shuai Yang: Conceptualization (lead); data curation (lead); investigation (lead); software (lead); writing – original draft (lead); writing – review and editing (equal). **Yang He:** Investigation (supporting); supervision (supporting); writing – review and editing (equal). **Jinsong Leng:** Funding acquisition (lead); supervision (lead); writing – review and editing (supporting).

ACKNOWLEDGMENTS

This work was supported by the National Natural Science Foundation of China (Grant No. 11632005), and Heilongjiang Touyan Innovation Team Program. The SAXS experiments were carried out at beamline BL19U2 of Shanghai Synchrotron Radiation Facility (SSRF).

DATA AVAILABILITY STATEMENT

Research data are not shared.

ORCID

Jinsong Leng  <https://orcid.org/0000-0001-5098-9871>

REFERENCES

- [1] X. Liu, L. Zhao, F. F. Liu, D. Astruc, H. B. Gu, *Coord. Chem. Rev.* **2020**, *419*, 213406.
- [2] C. J. Zeng, L. W. Liu, W. F. Bian, Y. J. Liu, J. S. Leng, *Compos. B: Eng.* **2020**, *194*, 108034.
- [3] X. Wan, L. Luo, Y. J. Liu, J. S. Leng, *Adv. Sci.* **2020**, *7*, 2001000.
- [4] W. N. Du, Y. Jin, L. J. Shi, Y. C. Shen, S. Q. Lai, Y. T. Zhou, *Compos. B: Eng.* **2020**, *195*, 108092.
- [5] Y. Chen, X. Zhao, C. Luo, Y. Shao, M. B. Yang, B. Yin, *Compos. Part A: Appl. Sci. Manuf.* **2020**, *135*, 105931.
- [6] Z. X. Liu, X. Lan, W. F. Bian, L. W. Liu, Q. F. Li, Y. J. Liu, J. S. Leng, *Compos. B: Eng.* **2020**, *193*, 108056.
- [7] M. Y. Wu, P. Sukyai, D. Lv, F. Zhang, P. D. Wang, C. Liu, B. Li, *Chem. Eng. J.* **2020**, *392*, 123673.
- [8] T. W. Wong, M. Behl, N. I. S. M. Yusoff, T. F. Li, M. U. Wahit, A. F. Ismail, Q. Zhao, A. Lendlein, *Compos. Sci. Technol.* **2020**, *194*, 108138.

- [9] J. C. Worch, A. C. Weems, J. Y. Yu, M. C. Arno, T. R. Wilks, R. T. R. Huckstepp, R. K. O'Reilly, M. L. Becker, A. P. Dove, *Nat. Commun.* **2020**, *11*, 3250.
- [10] Q. Zhou, X. L. Dong, Y. X. Xiong, B. B. Zhang, S. Lu, Q. Wang, Y. G. Liao, Y. J. Yang, H. Wang, *ACS Appl. Mater. Interfaces* **2020**, *12*, 28539.
- [11] R. Xiao, W. M. Huang, *Macromol. Sci.* **2020**, *20*, 2000108.
- [12] H. Garg, J. Mohanty, P. Gupta, A. Das, B. P. Tripathi, B. Kumar, *Macromol. Mater. Eng.* **2020**, *305*, 2000215.
- [13] X. F. Li, X. Y. Peng, R. Z. Li, Y. K. Zhang, Z. F. Liu, Y. W. Huang, S. J. Long, H. Y. Li, *Macromol. Rapid Commun.* **2020**, *41*, 2000202.
- [14] F. H. Zhang, Y. L. Xia, Y. J. Liu, J. S. Leng, *Nanoscale Horiz.* **2020**, *5*, 1155.
- [15] X. Li, W. K. Liu, Y. M. Li, W. L. Lan, D. G. Zhao, H. C. Wu, Y. Feng, X. L. He, Z. Li, J. H. Li, F. Luo, H. Tan, *J. Mater. Chem. B* **2020**, *8*, 5117.
- [16] X. L. Pang, L. Qin, B. Xu, Q. Liu, Y. L. Yu, *Adv. Funct. Mater.* **2020**, *30*, 202002451.
- [17] F. Pilate, R. Mincheva, J. De Winter, P. Gerbaux, L. B. Wu, R. Todd, J. M. Raquez, P. Dubois, *Chem. Mater.* **2014**, *26*, 5860.
- [18] J. Yan, M. F. Li, Z. W. Wang, C. Chen, C. Q. Ma, G. Yang, *Chem. Eng. J.* **2020**, *389*, 123468.
- [19] A. S. Kuenstler, K. D. Clark, J. R. de Alaniz, R. C. Hayward, *ACS Macro Lett.* **2020**, *9*, 902.
- [20] X. L. Pang, J. A. Lv, C. Y. Zhu, L. Qin, Y. L. Yu, *Adv. Mater.* **2019**, *27*, 1904224.
- [21] Y. C. Li, H. T. Zhuo, H. Chen, S. J. Chen, *Polymer* **2019**, *179*, 121671.
- [22] M. Q. Xie, C. Wu, C. Y. Chen, Y. Liu, C. Z. Zhao, *Polym. Chem.* **2019**, *10*, 4852.
- [23] B. Wang, K. F. Chen, R. D. Yang, F. Yang, J. Liu, *Carbohydr. Polym.* **2014**, *103*, 510.
- [24] B. Wang, K. F. Chen, R. D. Yang, F. Yang, J. Liu, *J. Appl. Polym. Sci.* **2014**, *131*, 40288.
- [25] A. C. Fonseca, M. S. Lima, A. F. Sousa, A. J. Silvestre, J. F. J. Coelho, A. C. Serra, *Polym. Chem.* **2019**, *10*, 1696.
- [26] K. J. Wang, Y. G. Jia, X. X. Zhu, A. C. S. Biomater, *Sci. Eng.* **2015**, *1*, 855.
- [27] N. Kawatsuki, R. Fujii, Y. Fujioka, S. Minami, M. Kondo, *Langmuir* **2017**, *33*, 2427.
- [28] M. H. Wang, J. C. Kim, *Colloid Polym. Sci.* **2014**, *292*, 965.
- [29] H. Y. Du, J. H. Zhang, *Sensor. Actuat. A: Phys.* **2012**, *179*, 114.
- [30] L. Wang, X. F. Yang, H. M. Chen, T. Gong, W. B. Li, G. Yang, S. B. Zhou, *ACS Appl. Mater. Interfaces* **2013**, *5*, 10520.
- [31] A. Kausar, *J. Plast. Film Sheet.* **2018**, *34*, 256.
- [32] H. Yang, W. R. Leow, T. Wang, J. Wang, J. C. Yu, K. He, D. P. Qi, C. J. Wan, X. D. Chen, *Adv. Mater.* **2017**, *29*, 1701627.
- [33] E. S. Keneth, R. Lieberman, M. Rednor, G. Scalet, F. Auricchio, S. Magdassi, *Polymer* **2020**, *12*, 710.
- [34] X. D. Qi, Y. W. Shao, H. Y. Wu, J. H. Yang, Y. Wang, *Compos. Sci. Technol.* **2019**, *181*, 107714.
- [35] S. R. Mishra, J. B. Tracy, *ACS Appl. Nano Mater.* **2018**, *1*, 3063.
- [36] Q. Y. Guo, C. J. Bishop, R. A. Meyer, D. R. Wilson, L. Olasov, D. E. Schlesinger, P. T. Mather, J. B. Spicer, J. H. Elisseeff, J. J. Green, *ACS Appl. Mater. Interfaces* **2018**, *10*, 13333.
- [37] S. T. Li, X. Z. Jin, Y. W. Shao, X. D. Qi, J. H. Yang, Y. Wang, *Eur. Polym. J.* **2019**, *116*, 302.
- [38] X. Cao, H. Z. Liu, X. H. Yang, J. H. Tian, B. H. Luo, M. X. Liu, *Compos. Sci. Technol.* **2020**, *191*, 108071.
- [39] H. Y. Wu, R. T. Chen, Y. W. Shao, X. D. Qi, J. H. Yang, Y. Wang, *ACS Sustain. Chem. Eng.* **2019**, *7*, 13532.
- [40] L. Yang, R. Tong, Z. H. Wang, H. S. Xia, *ChemPhysChem* **2018**, *19*, 2052.
- [41] K. Yan, F. Y. Xu, C. Y. Wang, Y. Y. Li, Y. L. Chen, X. F. Li, Z. T. Lu, D. Wang, *Biomater. Sci.* **2020**, *8*, 3193.
- [42] F. Ji, X. D. Liu, D. K. Sheng, Y. M. Yang, *Polymer* **2020**, *197*, 122514.
- [43] G. Scalet, *Actuators* **2020**, *9*, 10.
- [44] D. Ren, Y. J. Chen, H. Li, H. UrRehman, Y. L. Cai, H. Z. Liu, *Colloid. Surface. A* **2019**, *580*, 123731.
- [45] A. Lendlein, H. Y. Jiang, O. Jünger, R. Langer, *Nature* **2005**, *434*, 879.
- [46] C. M. Tuan, V. D. C. Tinh, D. Kim, *Membranes* **2020**, *10*, 138.
- [47] X. F. Li, K. Q. Wang, D. Liu, L. M. Lin, J. H. Pang, *Polymer* **2020**, *195*, 122456.
- [48] W. C. Liu, Z. Wang, X. M. Du, J. M. Xu, C. Liu, H. Q. Li, Z. Y. Chen, C. M. Wang, H. Chen, L. Chen, *ACS Sustain. Chem. Eng.* **2020**, *8*, 6505.
- [49] Z. Y. Chen, Z. Wang, L. Hou, C. M. Wang, X. M. Du, C. Liu, W. C. Liu, H. Q. Li, *J. Polym. Res.* **2019**, *26*, 267.
- [50] J. M. Xu, Z. G. Zhang, K. Yang, W. W. He, X. D. Yang, X. M. Du, L. X. Meng, P. Y. Zhao, Z. Wang, *J. Membr. Sci.* **2020**, *596*, 117711.
- [51] H. Li, D. W. Luo, J. L. He, F. Lin, H. Wang, L. Yu, W. Liu, J. Li, *CrystEngComm* **2020**, *22*, 1577.
- [52] X. M. Du, Z. Wang, W. C. Liu, J. M. Xu, Z. Y. Chen, C. M. Wang, *J. Membr. Sci.* **2018**, *566*, 205.
- [53] Y. Lu, X. T. Pan, N. Li, Z. X. Hu, S. W. Chen, *Appl. Surf. Sci.* **2020**, *503*, 144071.
- [54] J. S. Li, S. Wang, F. X. Liu, X. Wang, H. Chen, T. J. Mao, Z. Wang, *J. Membr. Sci.* **2019**, *581*, 303.

SUPPORTING INFORMATION

Additional supporting information can be found online in the Supporting Information section at the end of this article.

How to cite this article: S. Yang, Y. He, J. Leng, *J. Appl. Polym. Sci.* **2023**, e54444. <https://doi.org/10.1002/app.54444>